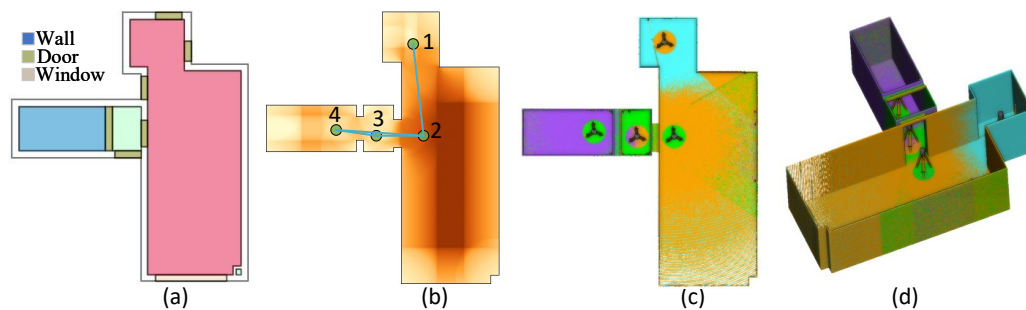


## Graphical Abstract

### VF-Plan: Bridging the Art Gallery Problem and Static LiDAR Scanning with Visibility Field Optimization

Biao Xiong, Longjun Zhang, Ruiqi Huang, Junwei Zhou, Bojian Wu, Fashuai Li



Viewpoint optimization for static LiDAR Scanning. (a) The input floor plan; (b) Optimized viewpoints indicated by green dots, with the Visibility Field displayed as the background image; (c) and (d) Simulated LiDAR points from optimal viewpoints, shown in 2D and 3D respectively, with each scan distinguished by a unique color.

## Highlights

### **VF-Plan: Bridging the Art Gallery Problem and Static LiDAR Scanning with Visibility Field Optimization**

Biao Xiong, Longjun Zhang, Ruiqi Huang, Junwei Zhou, Bojian Wu, Fashuai Li

- **Unified Solution to VPP and AGP:** Our method addresses the combined challenges of viewpoint planning and the Art Gallery Problem, achieving efficient coverage with minimal viewpoints and robust network connectivity.
- **Visibility Field for Dimensionality Reduction:** We introduce a continuous Visibility Field tailored to static LiDAR systems, reducing the optimization space from 2D to 1D by leveraging structural elements like medial axis and joints.
- **Greedy Algorithm for Efficient Coverage:** Our greedy Algorithm utilizes the VF's structural insights to construct a minimal, fully connected viewpoint network, ensuring both robust coverage and network connectivity.

# VF-Plan: Bridging the Art Gallery Problem and Static LiDAR Scanning with Visibility Field Optimization

Biao Xiong<sup>a</sup>, Longjun Zhang<sup>a</sup>, Ruiqi Huang<sup>a</sup>, Junwei Zhou<sup>a</sup>, Bojian Wu<sup>b</sup>,  
Fashuai Li<sup>c,\*\*</sup>

<sup>a</sup>*School of Computer Science and Artificial Intelligence, Wuhan University of  
Technology, 122 Luoshi Rd, Wuhan, 430070, Hubei, China*

<sup>b</sup>*College of Computer Science and Technology, Zhejiang University, 866 Yuhangtang  
Rd, Hangzhou, 310058, Zhejiang, China*

<sup>c</sup>*The Advanced Laser Technology Laboratory of Anhui Province, 850 Huangshan  
Rd, Hefei, 230031, Anhui, China*

---

## Abstract

Viewpoint planning is crucial for 3D data collection and autonomous navigation, yet existing methods often miss key optimization objectives for static LiDAR, resulting in suboptimal network designs. The Viewpoint Planning Problem (VPP), which builds upon the Art Gallery Problem (AGP), requires not only full coverage but also robust registrability and connectivity under limited sensor views. We introduce a greedy optimization algorithm that tackles these VPP and AGP challenges through a novel **Visibility Field (VF)** approach. The VF captures visibility characteristics unique to static LiDAR, enabling a reduction from 2D to 1D by focusing on medial axis and joints. This leads to a minimal, fully connected viewpoint network with comprehensive coverage and minimal redundancy. Experiments across diverse environments show that our method achieves high efficiency and scalability, matching or surpassing expert designs. Compared to state-of-the-art methods, our approach achieves comparable viewpoint counts (VC) while reducing Weighted Average Path Length (WAPL) by approximately 95%, indicating a much more compact and connected network. Dataset and source code will be released upon acceptance.

---

\*E-mail addresses: b.xiong@whut.com (B. Xiong), 761427262z@gmail.com (L. Zhang), 2422440491@qq.com (R. Huang), junweizhou@whut.edu.cn (J. Zhou), ustcbjwu@gmail.com (B. Wu), lifashuai@gmail.com (F. Li).

\*\*Corresponding author.

*Keywords:* Viewpoint Optimization, Terrestrial Laser Scanning, Visibility Field, Medial axis transform, Greedy searching, BIM

---

## 1. Introduction

The Viewpoint Planning Problem (VPP) has emerged as a critical research spot due to the growing use of LiDAR and camera sensors in applications such as 3D reconstruction, autonomous navigation, and Scan-to-BIM applications [41, 30]. VPP focuses on determining the optimal placements and configurations of sensors to achieve specific reconstruction goals, such as maximizing observation completeness and minimizing occlusions, while balancing efficiency and data quality. Both model-free and model-based algorithms for viewpoint and path planning have gained significant attention due to their applicability across various industries, including robotics, construction, and surveillance [31].

Conceptually, VPP is rooted in the Art Gallery Problem (AGP), a classic challenge in computational geometry that seeks the minimal number of “guards” required to cover a given area, typically a polygon, with full 360° visibility [25]. AGP is often simplified by constraining guard placements to polygon vertices; however, this simplification does not capture the true computational complexity of the problem. In its generalized form, AGP is  $\exists\mathbb{R}$ -complete, meaning it is at least as hard as any NP-complete problem, with no known efficient solutions [11, 1]. This NP-hard nature has inspired substantial research interest, particularly in constrained versions that make idealized assumptions, such as complete visibility and static scenes [11, 41].

VPP, however, introduces additional complexities beyond those of AGP. Unlike static guards, sensors in VPP must maintain overlapping fields of view for accurate data registration, accommodate limited and directional visibility ranges, and meet high accuracy requirements for 3D scene reconstruction. These real-world demands, especially in cluttered or partially obstructed environments, render VPP a more challenging NP-hard problem, requiring innovative optimization strategies beyond those used for AGP [41, 1].

Our work addresses these challenges by introducing a novel greedy approach based on the concept of a *Visibility Field (VF)*, specifically designed for static LiDAR applications. The VF captures the unique visibility characteristics of LiDAR, including constraints on range and incident angles, enabling a significant reduction in computational complexity. By focusing

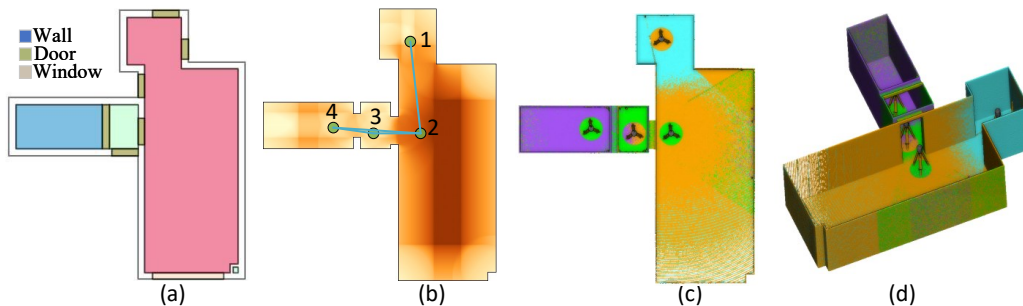


Figure 1: Viewpoint optimization for static LiDAR Scanning. (a) The input floor plan; (b) Optimized viewpoints indicated by green dots, with the Visibility Field displayed as the background image; (c) and (d) Simulated LiDAR points from optimal viewpoints, shown in 2D and 3D respectively, with each scan distinguished by a unique color.

on critical points such as medial axis and joints within the VF, we effectively reduce the optimization space from 2D to 1D, facilitating the construction of a minimal, fully connected viewpoint network that achieves comprehensive coverage with reduced redundancy. Our main contributions are as follows:

1. **Unified Solution to VPP and AGP:** Our method addresses the combined challenges of viewpoint planning and the Art Gallery Problem, achieving efficient coverage with minimal viewpoints and robust network connectivity.
2. **Visibility Field for Dimensionality Reduction:** We introduce a continuous Visibility Field tailored to static LiDAR systems, reducing the optimization space from 2D to 1D by leveraging structural elements like medial axis and joints.
3. **Greedy Algorithm for Efficient Coverage:** Our greedy algorithm utilizes the VF’s structural insights to construct a minimal, fully connected viewpoint network, ensuring both robust coverage and network connectivity.

## 2. Related Work

This section reviews key advancements in sensor network planning, covering both static and mobile sensing, with a focus on recent works in LiDAR

and computer vision area. These serve as the foundation for the viewpoint planning method proposed here, addressing gaps in efficient coverage, connectivity, and optimization complexity.

### *2.1. Station-Based Scanning*

Sensor network design shares similarities with the Planning for Scanning (P4S) problem, observed in applications like surveillance cameras [32, 55, 16], directional sensors [15], 5G base stations [42, 45], stealth game [49], and station-based LiDAR scanning [2]. For LiDAR, the goal is to cover the entire scene with comprehensive wall scanning while ensuring data quality criteria such as completeness and accuracy [29, 2].

Advancements in LiDAR technology have led to P4S methods using prior information like 2D drawings and 3D models [29]. These methods have been applied to civil infrastructures [50], space frame structures [29], rebar detection [27, 28], and landslide monitoring [54]. In cases where prior information is outdated or unavailable, low-resolution preliminary scans are required, either indoors [39] or outdoors using UAVs [26].

P4S optimizations aim to maximize coverage and overlap while minimizing the number of viewpoints [19, 7]. Methods like CMA Evolution Strategy [40] and regular grid sampling [21, 33] increase the likelihood of finding optimal viewpoints but also raise computational complexity. Jia’s approach using grid-based sampling [20, 21, 22] scores candidate viewpoints based on observed wall segments, though this approach is limited by its reliance on reference objects for registration. Noichl [35] improve Jia’s method into 3D scene for an uniform covering by triangulating 3D scene into meshes and checking their visibility. For scenarios lacking BIM priors, structural elements can be surveyed and detected using low-cost sensors to serve as a preliminary prior for static station planning. A precise scan is then performed in a stop-and-go manner using a static scanner mounted on a robotic dog [9, 18].

Our approach addresses these limitations by using a continuous Visibility Field (VF) model, which reduces optimization from 2D to 1D by focusing on structural convergence points like medial axis and joints, thus minimizing computation and enhancing adaptability.

### *2.2. Mobile-Based Exploration*

Coverage Path Planning (CPP) focuses on computing optimal, collision-free paths for robots to fully cover target areas [44]. Techniques like Rapidly-

exploring Random Trees (RRT) and their variants (RRT\* [23], RRT# [37]) are widely used for autonomous exploration in unknown spaces, including UAVs [31] and wheeled robots [38]. RRT-based methods maximize information gain while minimizing travel distance [17, 47, 53].

Methods utilizing tensor fields for guiding robot movements enable efficient path routing in partially reconstructed indoor scenes [48, 46]. Recent approaches like the Signed Distance Field (SDF) and Hamilton-Jacobi skeleton further improve path planning in known environments [36]. These concepts share similarities with our visibility field, which leverages converging lines for efficient viewpoint planning.

For known environments, algorithms like the receding horizon "next-best-view" approach [3] and dual-resolution mapping schemes [6] balance detailed local mapping with efficient global exploration. For applications in autonomous driving and exploration, recent advances such as "LookOut" [12] propose diverse multi-future prediction models that enhance autonomous navigation by predicting possible trajectories, balancing safety, and efficiency.

### 3. Theoretical Foundations and Global Optimality

This section formulates the Viewpoint Planning Problem (VPP) for static LiDAR scanning in a 2D polygonal environment and establishes the theoretical basis for restricting candidate viewpoints to the *medial axis* (MA). We first present the problem definition, including coverage and connectivity requirements, and then show that any line segment visible from an interior point is also visible from a corresponding set of MA points. This demonstrates that restricting the viewpoint search space to the MA incurs no loss of coverage capability. Finally, we prove that a minimal solution confined to the MA is *globally optimal*.

#### 3.1. Problem Definition

Let  $P$  be a 2D polygonal region (such as a floor plan) with possible obstacles or holes, while remaining topologically connected. The polygon's boundary (including internal obstacles) is discretized into  $n$  small line segments:

$$L = \{l_1, l_2, \dots, l_n\},$$

which represent the target structures (e.g., walls or windows) to be covered by static LiDAR scanners (hereafter referred to as *viewpoints*).

*Candidate Viewpoints.* We aim to position a set of viewpoints such that all segments in  $L$  are fully visible, while the chosen viewpoints remain connected under an overlap criterion. Let  $V = \{v_1, v_2, \dots, v_m\}$  be the set of candidate viewpoint locations. We will later establish that it is sufficient to confine  $V$  to the *medial axis* of  $P$ , reducing a 2D search to a simpler 1D structure.

*Visibility.* we define a *Completeness Table*  $C$ , where  $C_{ij}$  indicates whether viewpoint  $V_i$  observes line segment  $L_j$

$$C_{ij} = \begin{cases} 1 & \text{if } v_i \text{ has an unobstructed view of } l_j \\ 0 & \text{otherwise} \end{cases} \quad (1)$$

*Connectivity via Overlap.* Consider any pair of viewpoints  $(v_i, v_k)$ . Let  $O_{ik}$  be their *overlap ratio*, i.e., the fraction of segments in  $L$  that both  $v_i$  and  $v_k$  can simultaneously observe. For a threshold  $\tau$ , an edge  $(v_i, v_k)$  exists in an *overlap graph*  $G = (V, E)$  if  $O_{ik} \geq \tau$ . A chosen subset  $S \subseteq V$  must then form a connected subgraph under this threshold.

*Mathematical Formulation.* We seek a minimal subset  $S \subseteq V$  of viewpoints such that:

- (a) *Coverage:* Each segment  $l_j \in L$  is observed by at least one viewpoint in  $S$ , i.e.,

$$\forall l_j \in L, \exists v_i \in S : C_{ij} = 1. \quad (2)$$

- (b) *Connectivity:* The induced subgraph  $(S, E_S)$  is connected under the overlap threshold  $\tau$ , where

$$E_S = \{(v_i, v_k) \in E \mid v_i, v_k \in S, O_{ik} \geq \tau\}. \quad (3)$$

The optimization problem becomes:

$$\min_{S \subseteq V} |S| \quad \text{subject to} \quad (2) \text{ and } (3). \quad (4)$$

Since problem (4) generalizes the set cover problem (with additional connectivity constraints), it remains NP-hard. Nonetheless, by restricting  $V$  to the medial axis (MA), we retain optimality while reducing the search complexity considerably.

### 3.2. Skeleton Completeness and Visibility Propagation

*Medial Axis (MA).* The MA of  $P$  is the set of points inside  $P$  that are equidistant to at least two boundary edges. In Blum’s *grassfire transform* [4], if the boundary of  $P$  is ignited simultaneously, the inward-propagating flames collide and form the locus of the MA.

**Theorem 1** (Skeleton Completeness). *Suppose an interior point  $p \in P$  sees a set of boundary segments  $L_p \subseteq L$ . Then there exists a set of points  $\{q_l\} \subseteq \text{MA}(P)$  such that*

$$L_p \subseteq \bigcup_{l \in L_p} \text{Vis}(q_l).$$

*Hence, for any interior coverage provided by  $p$ , there exists an MA-based set of points whose collective coverage reproduces that of  $p$ .*

**Sketch of Proof.** Using Blum’s “fire transformation,” the visibility from every segment propagates inward until it intersects the medial axis  $\text{MA}(P)$ . Each line segment  $l_j \in L_p$  must intersect  $\text{MA}(P)$  at some point  $q_j$  visible to  $l_j$ . Thus,

$$\text{Vis}(p) \subseteq \bigcup_{l_j \in \text{Vis}(p)} \text{Vis}(q_j).$$

Consequently, although a single point on the MA may not match  $p$ ’s entire coverage, a suitable collection of MA points can, illustrated in 2. Restricting  $V$  to  $\text{MA}(P)$  therefore does not diminish the achievable coverage.

### 3.3. Global Minimal Cover–Connectivity on the Skeleton

By Theorem 1, any coverage by interior points can be equivalently transferred to a suitable set of points on the medial axis. Hence, in the formulation (4), restricting  $V$  to  $\text{MA}(P)$  (including any branch or joint nodes) captures all feasible coverage solutions.

**Theorem 2** (Global Minimal Cover–Connectivity). *Let  $S^* \subseteq \text{MA}(P)$  be a minimal solution to (4) that covers all  $l_j \in L$  and satisfies the overlap-based connectivity requirement. Then  $S^*$  is irreducible (i.e., removing any  $v_i \in S^*$  breaks coverage or connectivity), and no smaller interior configuration can outperform  $S^*$ . Therefore,  $S^*$  is globally optimal.*

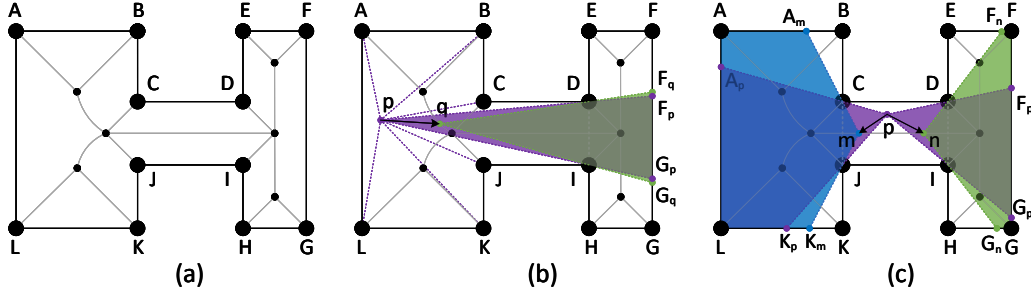


Figure 2: Illustration of skeleton completeness. (a) A simple polygon (black boundary) with its medial axis (gray arcs). (b) Coverage by an interior viewpoint  $p$  can be replicated by a single skeletal viewpoint  $q$  lying on the medial axis (MA). (c) In the general case, coverage from an interior viewpoint  $p$  may require multiple skeletal viewpoints (here,  $m$  and  $n$ ) to fully reproduce  $p$ 's visibility. Thus, no coverage capability is lost by restricting candidate viewpoints to the MA. For clarity, boundary segments commonly observed by both  $p$  and the MA viewpoints ( $q$ , or  $m$  and  $n$ ) are not drawn.

*Implication and Heuristic Search.* Exploiting the symmetry of the medial axis, no point *outside*  $MA(P)$  can provide superior coverage or connectivity. Consequently, a minimal cover-connectivity solution restricted to the skeleton cannot be improved by adding non-skeleton points. Hence, solving (4) directly on  $MA(P)$  yields a globally optimal arrangement in  $P$ . Although the problem remains NP-hard, standard polynomial-time greedy algorithm (e.g., [10]) often produce near-optimal results in practice. Once obtained, the minimal MA-based solution is irreducible, further affirming its global optimality for the entire polygon.

## 4. Method

### 4.1. Overview

Our proposed VF-Plan addresses the NP-hard complexity of the VPP through a greedy approach centered on the VF. Given a structural floor plan, VF-Plan constructs a Viewpoint Network (VPN) that achieves comprehensive coverage with minimal viewpoints, ensuring connectivity and registrability. Each viewpoint is selected to form a fully connected observation network, minimizing registration errors via Least Squares Fitting (LSF).

As illustrated in Figure 3, the VF-Plan pipeline starts from a floor plan with structural elements (walls, columns, doors, windows) and proceeds

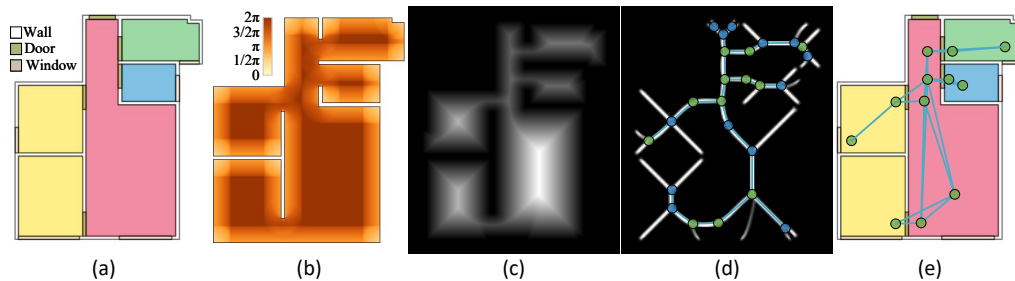


Figure 3: Overview of the Viewpoint Network (VPN) optimization based on the Visibility Field (VF). (a) Input floor plan; (b) Visibility Field (VF); (c) Distance field of VF; (d) Converging lines and points; (e) Optimized Viewpoint Network.

through the steps of VF computation, distance field generation, identification of medial axis and joint points, and initialization of candidate viewpoints. A greedy algorithm then refines these candidates into a minimal, connected VPN. To optimize the computationally intensive task of determining visible wall segments from each viewpoint, we employ a BSP-tree[14] to accelerate processing.

#### 4.2. Visibility Field

Laser scanning is limited to visible surfaces, leaving occluded areas unobserved. Therefore, visibility and coverage analysis are essential for viewpoint planning, with key objectives of maximizing observation completeness and registrability. The field of view is central to VPN optimization, defining the information captured at each viewpoint and guiding the selection of optimal viewpoints.

A common method for evaluating the information scanned by a LiDAR sensor is based on the length of observed walls [22]. Typically, wall length is counted either by ensuring both endpoints are visible or by partitioning walls into uniformly sampled segments within the scanner’s range. For 3D cases, visibility is evaluated by counting the number of observed voxels. However, these approaches lack normalization, yielding values that vary with discretization resolution and do not account for differences in distance or orientation to the scanner, impacting computational stability and load without improving coverage accuracy.

Our approach instead uses the valid scanned angle to integrate relevant factors into a single index, uniformly scaled from 0 to  $2\pi$ . We define a

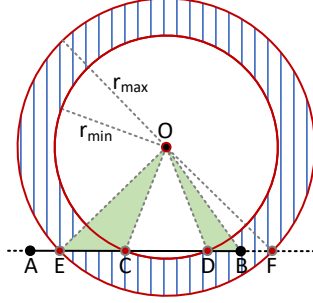


Figure 4: Scan model of a static scanner. The scanner provides valid observations within a  $360^\circ$  angle and a range from  $r_{\min}$  to  $r_{\max}$ .

static LiDAR scanner with a  $360^\circ$  field of view in the X-Y plane, a range from  $r_{\min}$  to  $r_{\max}$ , and uniform scanning speed, as shown in Figure 4. Only objects within this range are observable. Generally, closer viewpoints collect more information, but excessive proximity can occlude other parts of the field. Scanning is performed in discrete observation angles, with observed information defined as the valid observed angle, ensuring alignment with scanner properties.

To quantify observed data, let Circle\_min intersect line segment  $AB$  at points  $C$  and  $D$ , and Circle\_max at points  $E$  and  $F$ . The valid observed line segment is:

$$L_{\text{valid}} = \cap(L_{AB}, L_{EF}) - \cap(L_{AB}, L_{CD}) \quad (5)$$

and the corresponding observed angle is:

$$\theta_{\text{valid}} = \text{Angle}_O(L_{\text{valid}}) \quad (6)$$

Each viewpoint is assigned a View Angle, with the scene represented as a grid where each cell center is a viewpoint. Thus, the scene is represented as a Visibility Field, as shown in Figure 3(b), which aligns well with LiDAR properties and expert experience, displaying expected visibility patterns.

#### 4.3. Converging Lines and Joints

Observation data naturally converge to the medial axis and then joints of the Visibility Field, so placing viewpoints along these skeletons and joints ensures full coverage. Thus, VPN optimization reduces from a 2D to a 1D problem along these skeletons. We use an medial axis algorithm [43] to identify skeletons and joint points, placing candidate viewpoints along these

lines. Where overlap ratios are insufficient, additional viewpoints are added to ensure network cohesion.

For any skeleton ridge  $R_{ij}$  connecting joints  $J_i$  and  $J_j$ , we calculate an Overlap Ratio  $O_{ij}$  of the endpoints. When  $O_{ij}$  falls below a threshold, a midpoint  $J_m$  is added to split the ridge, ensuring connectivity. Both the skeleton joints and connecting points are called as converging points. And the resulting skeleton ridges are called converging lines. This iterative placement process continues until all converging points have adequate overlap for registrability.

#### 4.4. Overlap Ratio

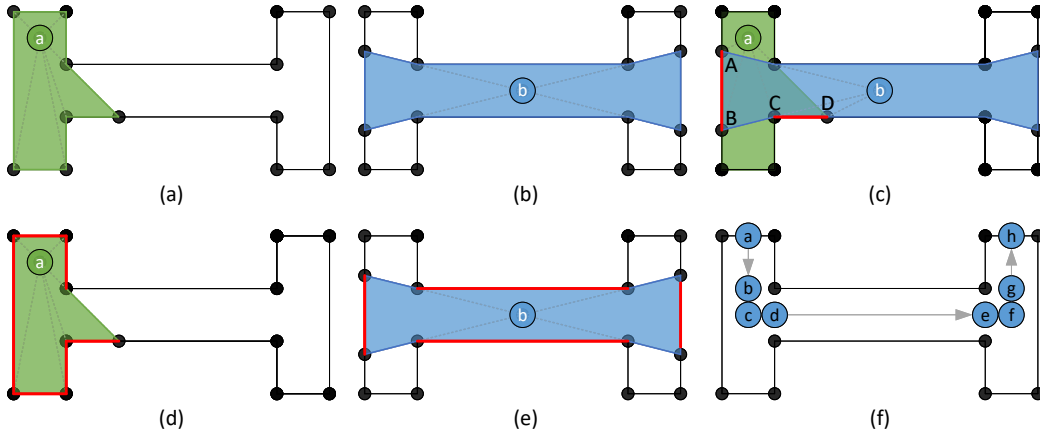


Figure 5: Overlap calculation between observed segments from different viewpoints, quantifying connectivity.

The Overlap Ratio quantifies shared visibility between viewpoints, a requirement for robust registration. Five overlap ratios based on length and angle are defined, ensuring effective connectivity independent of distance alone.

Given wall segments observed by viewpoint  $V_a$  as  $L_a$  with an observation angle  $\theta_a$ :

$$\theta_a = \text{Angle}(V_a, L_a) \quad (7)$$

The segments observed by both  $V_a$  and  $V_b$  are  $L_{ab}$ :

$$L_{ab} = L_a \cap L_b \quad (8)$$

The length-based overlap ratios are:

$$O^{\text{Min.Len}} = \frac{L_{ab}}{\min(L_a, L_b)} \quad (9)$$

$$O^{\text{Mean.Len}} = \frac{2L_{ab}}{L_a + L_b} \quad (10)$$

$$O^{\text{Union.Len}} = \frac{L_{ab}}{L_a \cup L_b} \quad (11)$$

And the angle-based overlap ratios are:

$$O^{\text{Union.Ang}} = \frac{\theta_a^{ab} + \theta_b^{ab}}{\theta_a + \theta_b} \quad (12)$$

$$O^{\text{Mean.Ang}} = \frac{\theta_a^{ab}}{2\theta_a} + \frac{\theta_b^{ab}}{2\theta_b} \quad (13)$$

#### 4.5. Greedy Optimization for VPN Construction

The VF-Plan greedy algorithm constructs an efficient Viewpoint Network (VPN) by starting with candidate viewpoints positioned strategically at key joints within the Visibility Field. For each pair of candidate viewpoints, an Overlap Ratio  $O$  is calculated, with pairs showing adequate overlap retained as adjacencies in the VPN to ensure robust connectivity.

To systematically track visibility, we construct the **Completeness Table  $C$**  (see Equation 1), which determines whether a given viewpoint  $v_i$  observes a specific line segment  $l_j$ . To enhance precision in observation tracking, wall boundaries are uniformly partitioned into equal-length segments.

As outlined in Algorithm 1 and illustrated in Figure 6, the greedy optimization initiates by selecting the viewpoint with the highest coverage as the seed. The algorithm then iteratively expands by adding neighboring viewpoints that maximize additional coverage, ensuring each new viewpoint significantly contributes to covering line segments while constructing a minimal, fully connected Viewpoint Network (VPN).

Upon completion of the initial search, the algorithm produces a single connected component encompassing all essential viewpoints, with sufficient overlap to facilitate stable connections. The algorithm subsequently enhances network stability by identifying cycles within the VPN graph. For nodes that cannot form cycles (i.e., loose nodes), Converging Points are added to ensure cohesion without redundancy. Additionally, any node with more than three connecting edges from a cycle selects a Converging Joint to establish loops, thereby strengthening network connectivity.

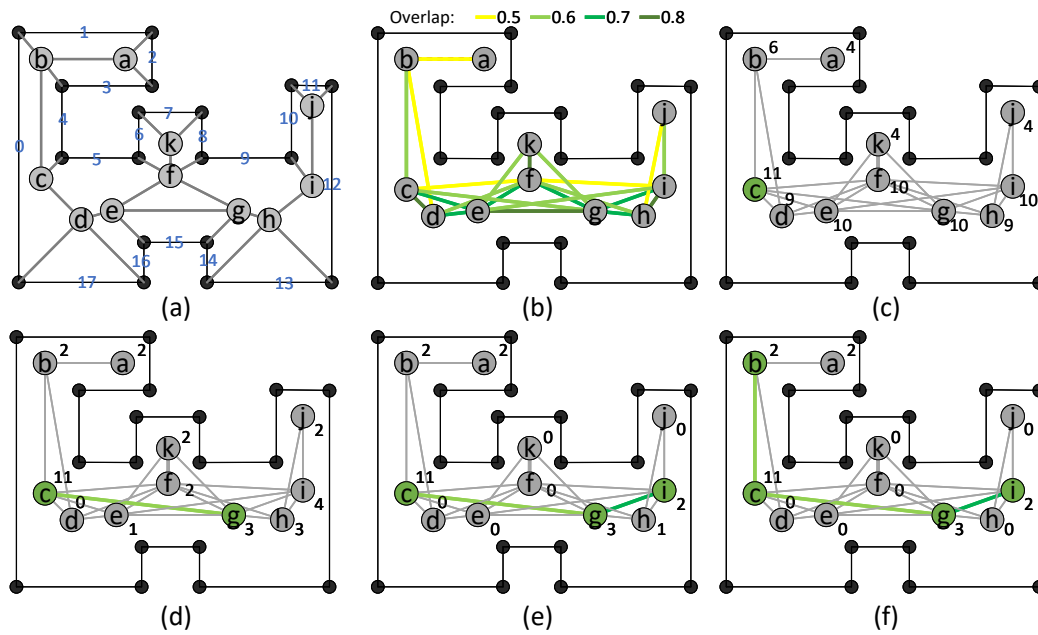


Figure 6: Greedy Optimization of VPN. (a) Floorplan showing candidate viewpoints (labeled a to k) positioned along walls (numbered 0 to 17); (b) Connectivity graph, where edges link viewpoints with overlap ratio  $O$  exceeding the threshold criterion; (c) Initial seed viewpoint selection based on maximum wall visibility (numbers near viewpoints indicate the count of observed walls); (d) - (f) Iterative expansion of the seed viewpoint set by adding adjacent viewpoints that provide the highest additional coverage, enhancing overall viewpoint arrangement.

---

**Algorithm 1** Greedy Optimization of VPN

---

**Input:** Candidate viewpoints  $V$ , line segments  $L$

**Output:** Minimal set of viewpoints  $V_{\text{opt}}$  covering all  $L$  and forming a connected network

1. Initialize Completeness Table  $C$
2. Identify  $V_i$  with maximum  $C_i$ , add  $V_i$  to Viewpoint Seed Set (VPS)
3. Add adjacent viewpoints of  $V_i$  to VPB
4. Remove all  $L$  observed by  $V_i$  from  $C$
5. **While** unobserved  $L$  exists in  $C$ :
  - (a) Select  $V_i$  in VPB maximizing new coverage  $C_i$
  - (b) If multiple options, select  $V_i$  with highest overlap  $O$  with VPS
  - (c) Move  $V_i$  to VPS, add adjacencies to VPB
  - (d) Remove all  $L$  observed by  $V_i$  from  $C$

**return** VPS as the optimized minimal VPN

---

## 5. Experiments

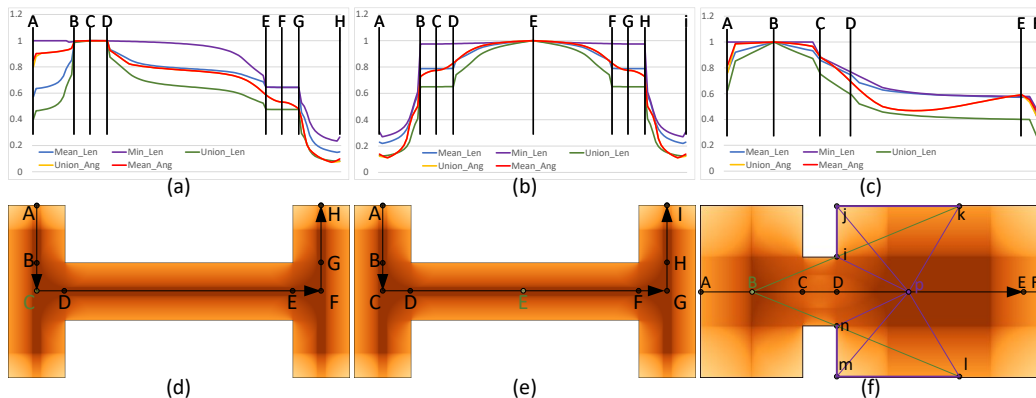


Figure 7: Performance of five proposed overlap ratios. The first row shows overlap ratios between moving and reference viewpoints; the second row illustrates room configurations, with black arrows indicating movement direction and green dots marking reference viewpoints.

### 5.1. Dataset

In this section, we evaluate the proposed VPN optimization algorithm across multiple scenarios and compare its performance with state-of-the-art methods in both indoor and outdoor environments.

Due to the lack of a dedicated benchmark for VPN optimization, we compiled a dataset from established sources, focusing on two primary scene types: indoor and outdoor environments. This dataset provides a robust foundation for evaluating VPN optimization across a range of realistic settings.

For indoor environments, we selected scenes with varied room layouts to evaluate the algorithm’s adaptability across multiple configurations. The Structure3D dataset [56] was included for its extensive collection of diverse Asian residential scenes, featuring both complex and compact room types frequently used in 3D modeling and synthetic data generation. VPNs generated from this dataset can also facilitate synthetic LiDAR data production for advancing research in 3D scene understanding. Specific scenes such as 00007, 00009, 00071, 02970, and 02972, discussed in subsequent sections, are drawn from Structure3D. For further comparisons, we incorporated additional scenes from Zeng1 [51], Noichl [34], Xu [48], and TUB1 from the ISPRS benchmark [52, 24].

For outdoor scenarios, we limited our approach to 2D site plans without considering terrain elevation, distinguishing our method from elevation-based approaches like [8]. Selected scenes include the CCIT and Crowsnest datasets from the University of Calgary [20] and the ECUT dataset from East China University of Technology [8], which represent open-space environments suitable for VPN optimization.

To evaluate VPN quality, we rely on expert-labeled annotations as standard ground truth data is unavailable. Where possible, we use existing expert-labeled VPNs (e.g., Zeng1, scene1 and TUB1), and for other cases, independent expert labels were created for comparison with manual designs.

### 5.2. Performance Metrics

The optimization algorithm aims to construct a minimal, fully connected viewpoint network with reduced redundancy. As most state-of-the-art methods achieve 100% coverage, we focus on two key metrics: the number of optimal viewpoints and network connectivity.

Network connectivity is measured using the **Weighted Average Path Length (WAPL)**, which reflects the compactness of the network [5]. A shorter WAPL indicates stronger connectivity and a more efficient structure. For a network with weighted edges  $w$ , WAPL is calculated as:

$$WAPL = \frac{1}{N(N-1)} \sum_{i \neq j} d_w(i, j) \quad (14)$$

where  $d_w(i, j)$  represents the shortest weighted path length between nodes  $i$  and  $j$ , and  $N$  is the total number of nodes.

The edge weight  $w$  is defined as

$$w_{ij} = 1 - O_{ij} \quad (15)$$

A larger  $O_{ij}$  implies stronger registration-based connectivity, meaning a shorter length between the two nodes  $i$  and  $j$ .

In cases where baseline methods do not yield a single connected component, some viewpoints may have a small overlap ratio with others. To ensure WAPL remains computable, we assign a large weight (100) to node pairs that lack a connecting path.

### 5.3. Algorithm Parameter Effects

#### 5.3.1. Overlap Ratio

We propose five overlap ratios according to the length of scanned walls and according angles to viewpoints in section 4.4. Here we evaluate them in two test indoor scenes, illustrated in Figure 7. Among them,  $O^{\text{Min.Len}}$  quickly reaches 100%, showing limited variability along movement paths, as seen from B to H in Figures 7(b) and (e), making it less suitable for dynamic scenes. The angle-based measures,  $O^{\text{Union.Ang}}$  and  $O^{\text{Mean.Ang}}$ , exhibit non-monotonic behavior, particularly along paths from C to E, shown in Figures 7(c) and (f), which limits their usefulness for consistent registration. The  $O^{\text{Union.Len}}$  measure tends to be too small, often underestimating connectivity. Therefore, we select  $O^{\text{Mean.Len}}$  for subsequent experiments and analyses due to its balanced performance across different scenarios.

#### 5.3.2. Scan Radius

The scan model used in this study operates in the X-Y plane with a 360° field of view, bounded by  $R_{\text{min}}$  and  $R_{\text{max}}$ , defining near and far blind zones. Typical static scanners, including the FARO M70, Trimble X7, and Leica BLK360, have maximum ranges around 40 meters and minimum ranges of about 1 meter, allowing for comprehensive indoor coverage but requiring precise placement in small rooms and narrow corridors.

For outdoor scenarios, we examine the impact of varying  $R_{\text{max}}$ , testing values at 15m, 30m, 45m, and 75m, with  $R_{\text{min}}$  fixed at 1m. As illustrated in Figure 8, increasing  $R_{\text{max}}$  expands the area of valid placements for viewpoints—defined where the View Angle exceeds 1.0—and reduces the Viewpoint Count (VC) needed for optimized coverage, from 23 to 14, 10, and 8. Larger  $R_{\text{max}}$  values are advantageous for open spaces, while smaller values require additional viewpoints for full coverage. These results indicate that our method aligns effectively with real-world scanner specifications and expert guidelines.

#### 5.3.3. Wall Partition

To improve station coverage accuracy, walls are partitioned into segments of varying lengths, as shown in Figure 9. We find that partitioning does not alter the final optimization result, but only affects the selection order of stations. Larger partition lengths (or no partitioning) place initial viewpoints at major intersections, optimizing computational cost and maintaining effective coverage.

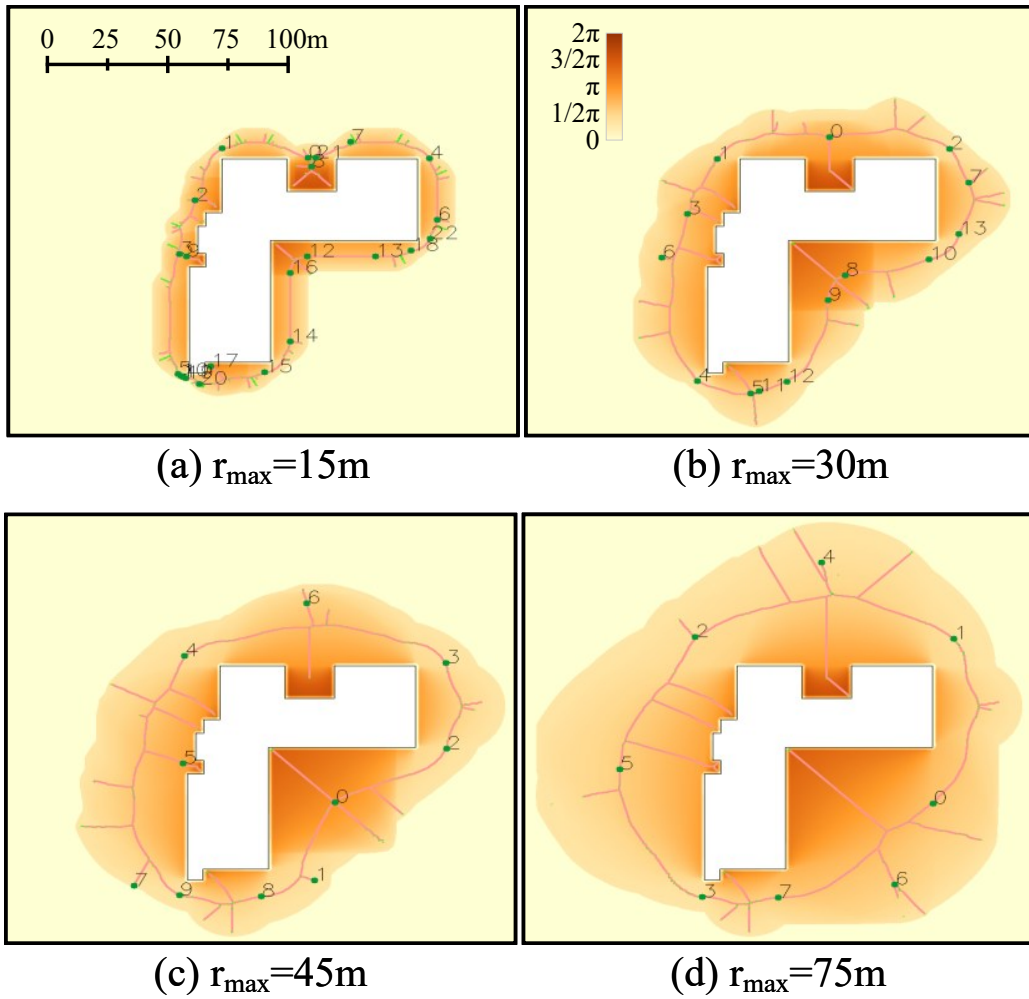


Figure 8: Effect of  $R_{\max}$  on Viewpoint Placement and Network Efficiency. As  $R_{\max}$  increases from 15m to 75m, the valid placement area (where View Angle  $> 1.0$ ) grows, reducing the Viewpoint Count (VC) needed for optimized VPN coverage from 23 to 8.

#### 5.3.4. Effect of Windows

Including windows in the model adds complexity to the skeleton structure, generating more detailed skeletons with additional joint points, as shown in Figure 10. When windows are considered, the VPN algorithm requires only a minimal increase in viewpoints to achieve complete coverage, as seen in Table 1.

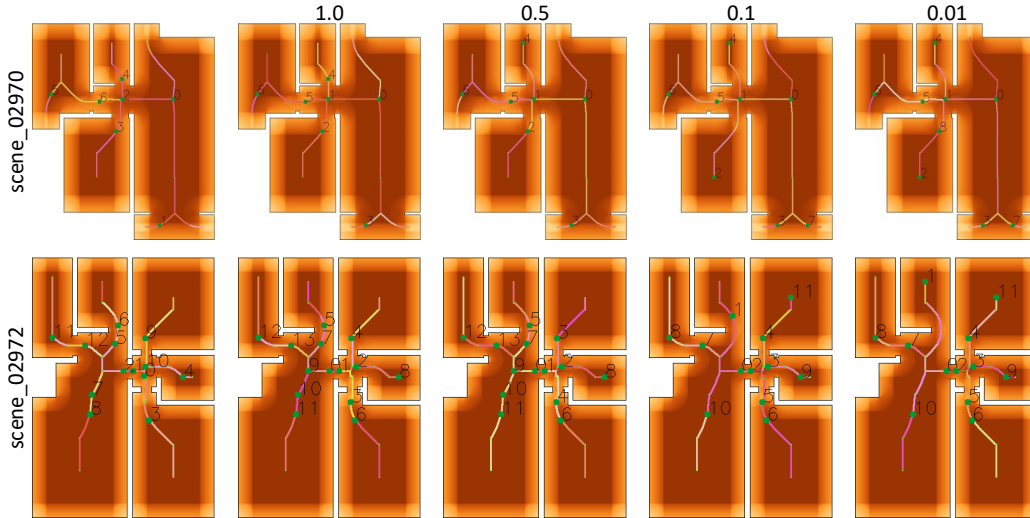


Figure 9: Effects of wall partitions. From left to right: unpartitioned walls and walls partitioned into segments of 1.0m, 0.5m, 0.1m, and 0.01m.

Without windows, the Viewpoint Count (VC) averages around 1.4 times the number of rooms, while with windows, it increases slightly to 1.6 times the room count. These results indicate that our algorithm effectively accommodates the added detail from windows. For precise window scans, including window frames in the optimization process is recommended.

Scene	00007	00009	00071
Number of Rooms	5	3	9
VC (Without Windows)	7	4	14
VC (With Windows)	7	5	15

Table 1: Viewpoint Count (VC) comparison for room coverage with and without windows across different scenes.

#### 5.4. Results and Analysis

We benchmarked our method against state-of-the-art approaches using datasets from prior studies, representing a range of indoor and outdoor scenes. Indoor datasets include Zeng1 [51], Noichl [34], and TUB1 from the ISPRS dataset [52]. Outdoor datasets consist of CCIT and Crowsnest

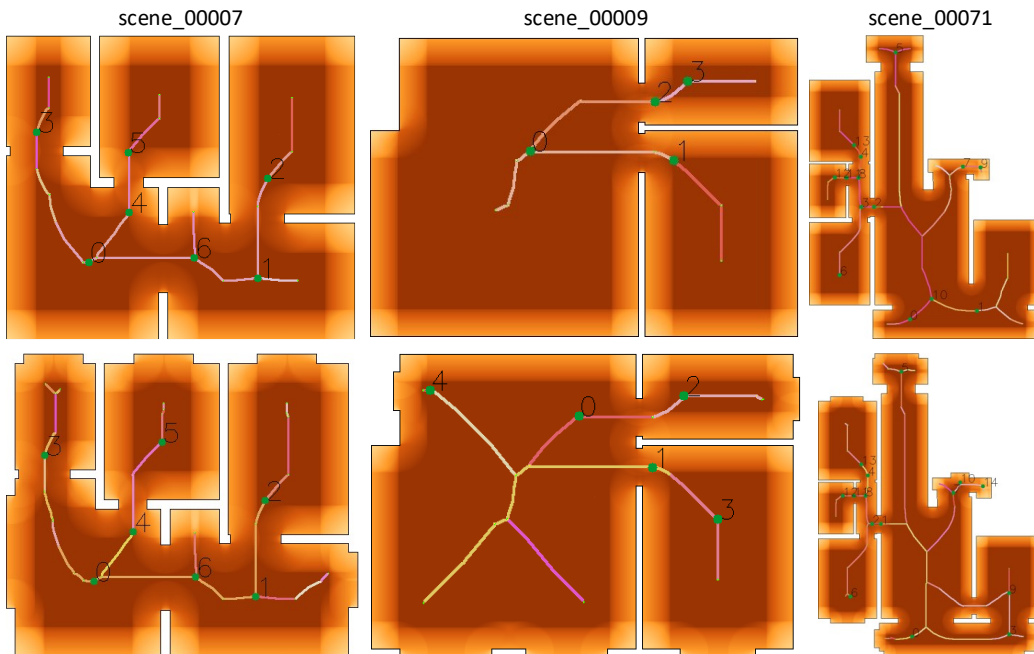


Figure 10: Comparison of VPN structures with and without windows. Including windows adds complexity to the skeleton and slightly increases the Viewpoint Count.

Scene	WAPL			VC			Baseline Method
	Expert	Ours	Baseline	Expert	Ours	Baseline	
Zeng1	0.47	0.53	43.37	12	12	10	Zeng[51]
Noichl	0.32	0.38	23.91	8	10	7	Noichl2023[34]
TUB1	1.03	1.00	40.97	28	29	19	Zhai2024[52]
Xu	0.35	0.31	28.69	8	8	7	Xu2017[48]
CCIT	0.52	0.47	38.12	8	8	7	Jia2018[20]
Crowsnest	0.50	0.49	34.02	9	8	8	Jia2018[20]
ECUT	0.67	0.76	11.94	58	52	139	Chen2023[8]

Table 2: Comparison of viewpoint counts (VC) and Weighted Average Path Length (WAPL) across indoor and outdoor scenes. Lower WAPL indicates more compact network connectivity.

from the University of Calgary [20] and ECUT from East China University of Technology [8].

**Indoor Results.** As shown in Figure 12, our method’s viewpoint opti-

mization closely aligns with expert-designed networks, achieving comprehensive coverage and creating compact, interconnected structures. This optimized network design enhances registration accuracy and connectivity, even in complex indoor settings.

**Outdoor Results.** For outdoor scenes, our method effectively adapts to open spaces, as illustrated in Figure 13. Adjustments to the  $R_{\max}$  parameter notably improved performance in expansive environments, reducing the required number of viewpoints without compromising coverage.

Table 2 demonstrates that our method performs comparably or better than expert-designed networks, achieving similar viewpoint counts (VC) and lower Weighted Average Path Length (WAPL). This outcome indicates a more compact and cohesive network structure. Unlike most baselines that often yield fragmented networks (highlighted by green ellipses in Figures 12 and 13), our approach maintains low WAPL scores, which reflect enhanced connectivity and minimized redundancy.

In indoor environments, our method achieves a 98% reduction in WAPL compared to baseline methods, creating highly connected networks well-suited for confined spaces. For complex outdoor scenarios, such as ECUT, our approach achieves a 91% WAPL reduction over baselines, demonstrating scalability and adaptability across both intricate indoor layouts and expansive outdoor scenes.

To further validate the optimized viewpoints, we simulated static LiDAR scanning at each optimized viewpoint using Helios++ [13]. As shown in Figure 11, the simulated LiDAR point clouds confirm complete scene coverage, with effective overlap between adjacent scans across both indoor and outdoor environments.

## 6. Conclusions

We introduced a novel solution to the Viewpoint Planning Problem and Art Gallery Problem in static LiDAR scanning by leveraging a Visibility Field to reduce optimization complexity from 2D to 1D. This VF-based approach enables the creation of a minimal, fully connected viewpoint network that ensures comprehensive coverage with reduced redundancy, advancing viewpoint planning for static LiDAR applications.

Our method offers a scalable and efficient framework applicable in structured and semi-structured environments, addressing real-world challenges in 3D data collection and autonomous navigation. Our VF framework adapts

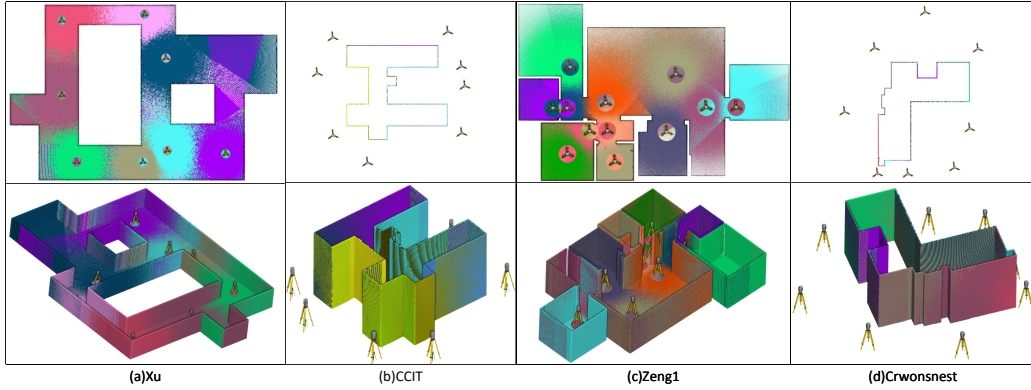


Figure 11: Simulated LiDAR points from optimal viewpoints. Each scan is uniquely colored. Top row shows top views, and bottom row shows oblique views with tripods indicating viewpoints.

well to real-world settings with potential obstructions by integrating partial occlusion handling based on initial scans.

In summary, this method provides a practical and robust solution for static viewpoint planning, with promising extensions to dynamic environments. Future work will focus on its application for large-scale LiDAR data collection and synthetic data generation, and expanding the method to support path planning in both 2D and 3D scenarios for more versatile deployment in complex environments.

### **CRedit authorship contribution statement**

Biao Xiong: Writing - Original draft, Validation, Methodology, Investigation, Project administration. Longjun Zhang: Original draft, Validation, Software, Methodology. Ruiqi Huang: Validation, Software, Methodology, Data curation. Junwei Zhou: Validation, Software, review & editing. Bojian Wu: Writing - review & editing, Writing - original draft, Visualization. Fashuai Li: Writing - review & editing, Supervision, Resources, Conceptualization.

### **Declaration of competing interest**

The authors declare that they have no known competing financial interests or personal relationships that could have appeared to influence the work

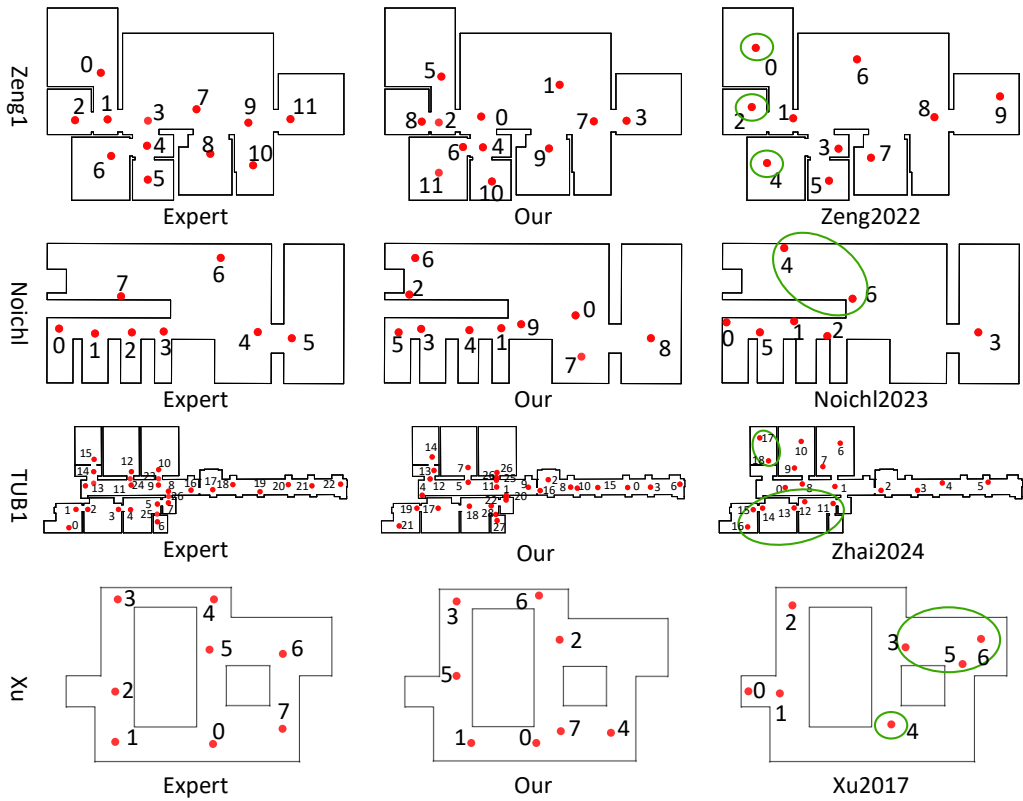


Figure 12: Viewpoint planning results for indoor environments. Red dots represent individual viewpoints, while green ellipses indicate clusters of viewpoints that are not connected to the main network.

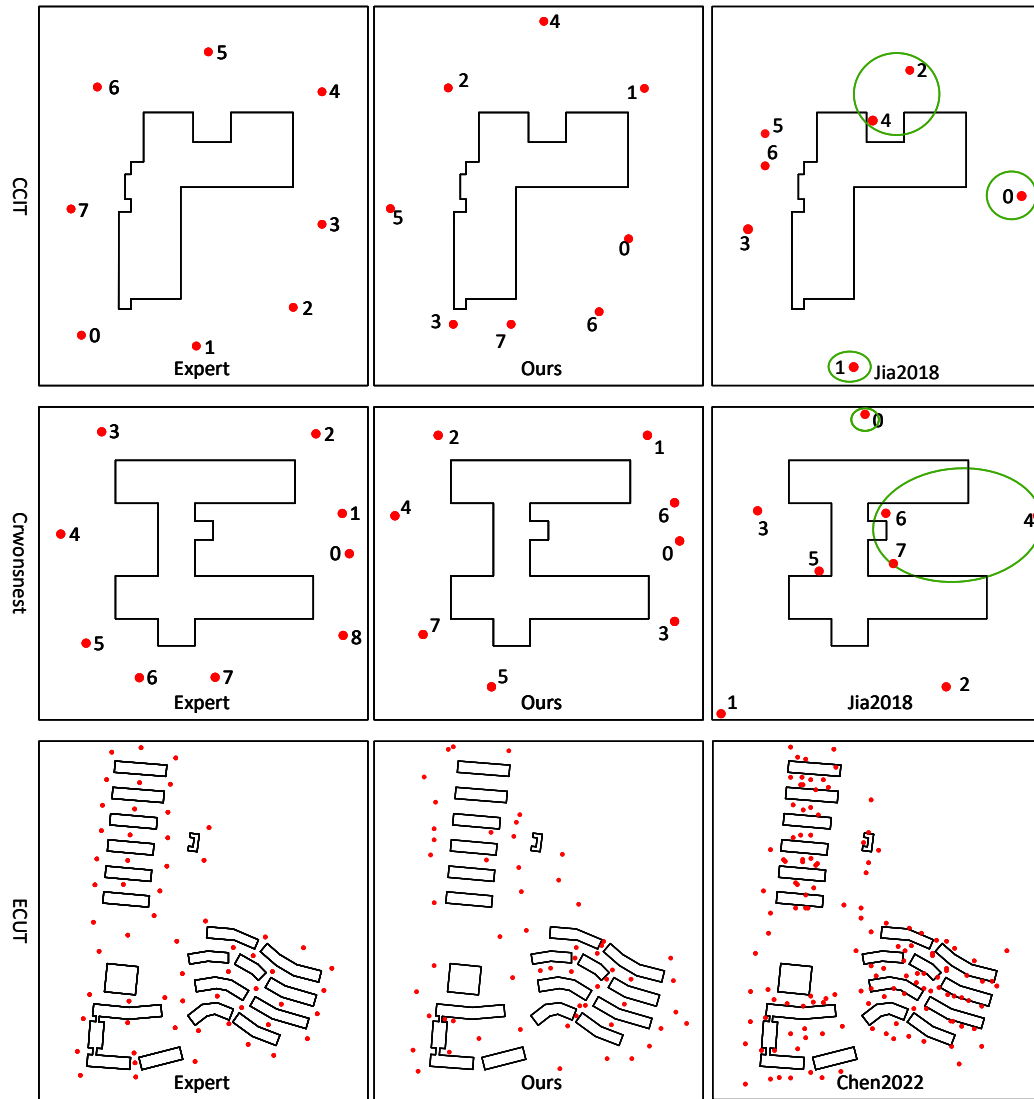


Figure 13: Viewpoint planning results for outdoor environments. Red dots represent individual viewpoints, while green ellipses indicate clusters of viewpoints that are not connected to the main network.

reported in this paper.

## References

- [1] Abrahamsen, M., Adamaszek, A., Miltzow, T., 2021. The art gallery problem is  $\exists\mathbb{R}$ -complete. *Journal of the ACM* 69, 1–70. doi:10.1145/3486655.
- [2] Aryan, A., Bosché, F., Tang, P., 2021. Planning for terrestrial laser scanning in construction: A review. *Automation in Construction* 125, 103551.
- [3] Bircher, A., Kamel, M., Alexis, K., Oleynikova, H., Siegwart, R., 2016. Receding horizon "next-best-view" planner for 3d exploration, in: 2016 IEEE International Conference on Robotics and Automation (ICRA), IEEE. pp. 1462–1468. doi:10.1109/ICRA.2016.7487276.
- [4] Blum, H., 1967. A transformation for extracting new descriptions of shape. *Models for the perception of speech and visual form* , 362–380.
- [5] Boccaletti, S., Latora, V., Moreno, Y., Chavez, M., Hwang, D.U., 2006. Complex networks: Structure and dynamics. *Physics reports* 424, 175–308.
- [6] Cao, C., Zhu, H., Ren, Z., Choset, H., Zhang, J., 2023. Representation granularity enables time-efficient autonomous exploration in large, complex worlds. *Science Robotics* 8, eadf0970. doi:10.1126/scirobotics.adf0970.
- [7] Chen, Z., Song, C., Wang, B., Tao, X., Zhang, X., Lin, F., Cheng, J.C., 2025. Automated reality capture for indoor inspection using bim and a multi-sensor quadruped robot. *Automation in Construction* 170, 105930.
- [8] Chen, Z., Zhang, W., Huang, R., Dong, Z., Chen, C., Jiang, L., Wang, H., 2022. 3d model-based terrestrial laser scanning (tls) observation network planning for large-scale building facades. *Automation in Construction* 144, 104594.

- [9] Chung, D., Kim, J., Paik, S., Im, S., Kim, H., 2025. Automated system of scaffold point cloud data acquisition using a robot dog. *Automation in Construction* 170, 105944.
- [10] Chvatal, V., 1979. A greedy heuristic for the set-covering problem. *Mathematics of operations research* 4, 233–235.
- [11] Couto, M.C., de Rezende, P.J., de Souza, C.C., 2011. An exact algorithm for minimizing vertex guards on art galleries. *International Transactions in Operational Research* 18, 425–448. doi:10.1111/j.1475-3995.2011.00800.x.
- [12] Cui, A., Casas, S., Sadat, A., Liao, R., Urtasun, R., 2021. Lookout: Diverse multi-future prediction and planning for self-driving, in: *Proceedings of the IEEE/CVF International Conference on Computer Vision*, pp. 16107–16116.
- [13] Esmorís, A.M., Yermo, M., Weiser, H., Winiwarter, L., Höfle, B., Rivera, F.F., 2022. Virtual lidar simulation as a high performance computing challenge: Toward hpc helios++. *IEEE Access* 10, 105052–105073. URL: <https://ieeexplore.ieee.org/document/9906068>, doi:<https://doi.org/10.1109/ACCESS.2022.3211072>.
- [14] Fuchs, H., Kedem, Z.M., Naylor, B.F., 1980. On visible surface generation by a priori tree structures, in: *Proceedings of the 7th annual conference on Computer graphics and interactive techniques*, pp. 124–133.
- [15] Fusco, G., Gupta, H., 2009. Selection and orientation of directional sensors for coverage maximization, in: *2009 6th Annual IEEE Communications Society Conference on Sensor, Mesh and Ad Hoc Communications and Networks*, IEEE. pp. 1–9. doi:10.1109/SAHCN.2009.5168945.
- [16] Ghanem, B., Cao, Y., Wonka, P., 2015. Designing camera networks by convex quadratic programming. *Computer Graphics Forum* 34, 77–88. doi:10.1111/cgf.12544.
- [17] Hepp, B., Nießner, M., Hilliges, O., 2018. Plan3d: Viewpoint and trajectory optimization for aerial multi-view stereo reconstruction. *ACM Transactions on Graphics (TOG)* 38, 1–17. doi:10.1145/3272127.

- [18] Hu, D., Gan, V.J., 2025. Semantic navigation for automated robotic inspection and indoor environment quality monitoring. *Automation in Construction* 170, 105949.
- [19] Ibrahim, A., Golparvar-Fard, M., El-Rayes, K., 2022. Metrics and methods for evaluating model-driven reality capture plans. *Computer-Aided Civil and Infrastructure Engineering* 37, 55–72. doi:10.1111/mice.12733.
- [20] Jia, F., Lichti, D.D., 2018. An efficient, hierarchical viewpoint planning strategy for terrestrial laser scanner networks, in: *ISPRS Annals of the Photogrammetry, Remote Sensing and Spatial Information Sciences*, pp. 137–144. doi:10.5194/isprs-annals-IV-2-137-2018.
- [21] Jia, F., Lichti, D.D., 2019. A model-based design system for terrestrial laser scanning networks in complex sites. *Remote Sensing* 11, 1749. doi:10.3390/rs11151749.
- [22] Jia, F., Lichti, D.D., 2022. A practical algorithm for the viewpoint planning of terrestrial laser scanners. *Geomatics* 2, 181–196. doi:10.3390/geomatics2020013.
- [23] Karaman, S., Frazzoli, E., 2011. Incremental sampling-based algorithms for optimal motion planning. *Robotics Science and Systems (RSS)* doi:10.15607/rss.2011.v7.021.
- [24] Khoshelham, K., Tran, H., Acharya, D., Vilariño, L.D., Kang, Z., Dallyot, S., 2021. Results of the isprs benchmark on indoor modelling. *ISPRS Open Journal of Photogrammetry and Remote Sensing* 2, 100008.
- [25] Lee, D., Lin, A., 1986. Computational complexity of art gallery problems. *IEEE Transactions on Information Theory* 32, 276–282. doi:10.1109/TIT.1986.1057160.
- [26] Li, D., Liu, J., Zeng, Y., Cheng, G., Dong, B., Chen, Y.F., 2022. 3d model-based scan planning for space frame structures considering site conditions. *Automation in Construction* 140, 104363. doi:10.1016/j.autcon.2022.104363.

- [27] Li, F., Kim, M.K., Lee, D.E., 2021. Geometrical model-based scan planning approach for the classification of rebar diameters. *Automation in Construction* 130, 103848. doi:10.1016/j.autcon.2021.103848.
- [28] Li, F., Kim, M.K., Sim, S.H., Chi, H.L., Lee, D.E., 2025. Full-scale application of dimensional quality assessment on precast slabs: A scan planning approach. *Measurement* 242, 115850.
- [29] Liu, J., Xu, D., Hyyppä, J., Liang, Y., 2021. A survey of applications with combined bim and 3d laser scanning in the life cycle of buildings. *IEEE Journal of Selected Topics in Applied Earth Observations and Remote Sensing* 14, 5627–5637.
- [30] Ma, Z., Liu, Y., Li, J., 2023. Review on automated quality inspection of precast concrete components. *Automation in Construction* 150, 104828.
- [31] Maboudi, M., Homaei, M., Song, S., Malihi, S., Saadatseresht, M., Gerke, M., 2023. A review on viewpoints and path planning for uav-based 3d reconstruction. *IEEE Journal of Selected Topics in Applied Earth Observations and Remote Sensing* 16, 5026–5048. doi:10.1109/JSTARS.2023.3269826.
- [32] Morsly, Y., Aouf, N., Djouadi, M.S., Richardson, M., 2011. Particle swarm optimization-inspired probability algorithm for optimal camera network placement. *IEEE Sensors Journal* 12, 1402–1412. doi:10.1109/JSEN.2011.2171706.
- [33] Noichl, F., Borrmann, A., 2022. Towards multicriterial scan planning in complex 3d environments, in: *International Conference on Computing in Civil and Building Engineering*, Springer. pp. 223–235.
- [34] Noichl, F., Borrmann, A., 2023. Automated deterministic model-based indoor scan planning, in: *ECPPM 2022-eWork and eBusiness in Architecture, Engineering and Construction 2022*. CRC Press, pp. 559–566.
- [35] Noichl, F., Lichti, D.D., Borrmann, A., 2024. Automating adaptive scan planning for static laser scanning in complex 3d environments. *Automation in Construction* 165, 105511.

- [36] Noël, T., Lehuger, A., Marchand, E., Chaumette, F., 2023. Skeleton disk-graph roadmap: A sparse deterministic roadmap for safe 2d navigation and exploration. *IEEE Robotics and Automation Letters* 9, 555–562. doi:10.1109/LRA.2023.3236339.
- [37] Otte, M., Frazzoli, E., 2015. Rrt<sup>x</sup> rrt<sup>x</sup>: Real-time motion planning/replanning for environments with unpredictable obstacles, in: *Algorithmic foundations of robotics XI: selected contributions of the eleventh international workshop on the algorithmic foundations of robotics*, Springer. pp. 461–478.
- [38] Placed, J.A., Strader, J., Carrillo, H., Atanasov, N., Indelman, V., Carlone, L., Castellanos, J.A., 2023. A survey on active simultaneous localization and mapping: State of the art and new frontiers. *IEEE Transactions on Robotics* 39, 1686–1705.
- [39] Qiu, Q., Wang, M., Tang, X., Wang, Q., 2021. Scan planning for existing buildings without bim based on user-defined data quality requirements and genetic algorithm. *Automation in Construction* 130, 103841.
- [40] Rougeron, G., Le Garrec, J., Andriot, C., 2022. Optimal positioning of terrestrial lidar scanner stations in complex 3d environments with a multiobjective optimization method based on gpu simulations. *ISPRS Journal of Photogrammetry and Remote Sensing* 193, 60–76.
- [41] Scott, W.R., Roth, G., Rivest, J.F., 2003. View planning for automated three-dimensional object reconstruction and inspection. *ACM Computing Surveys (CSUR)* 35, 64–96.
- [42] Shi, L., Shi, D., Zhang, X., Meunier, B., Zhang, H., Wang, Z., Vladimirescu, A., Li, W., Zhang, Y., Cosmas, J., et al., 2020. 5g internet of radio light positioning system for indoor broadcasting service. *IEEE Transactions on Broadcasting* 66, 534–544.
- [43] Siddiqi, K., Pizer, S., 2008. *Medial representations: mathematics, algorithms and applications*. volume 37. Springer Science & Business Media.
- [44] Tan, C.S., Mohd-Mokhtar, R., Arshad, M.R., 2021. A comprehensive review of coverage path planning in robotics using classical and heuristic algorithms. *IEEE Access* 9, 119310–119342.

- [45] Wang, Q., Zhao, X., Lv, Z., Ma, X., Zhang, R., Lin, Y., 2020. Optimizing the ultra-dense 5g base stations in urban outdoor areas: Coupling gis and heuristic optimization. *Sustainable Cities and Society* 63, 102445.
- [46] Xi, Y., Zhu, C., Duan, Y., Yi, R., Zheng, L., He, H., Xu, K., 2024. Thp: Tensor-field-driven hierarchical path planning for autonomous scene exploration with depth sensors. *Computational Visual Media* , 1–15.
- [47] Xie, K., Yang, H., Huang, S., Lischinski, D., Christie, M., Xu, K., Gong, M., Cohen-Or, D., Huang, H., 2018. Creating and chaining camera moves for quadrotor videography. *ACM Transactions on Graphics (TOG)* 37, 1–13.
- [48] Xu, K., Zheng, L., Yan, Z., Yan, G., Zhang, E., Niessner, M., Deussen, O., Cohen-Or, D., Huang, H., 2017. Autonomous reconstruction of unknown indoor scenes guided by time-varying tensor fields. *ACM Transactions on Graphics (TOG)* 36, 1–15.
- [49] Xu, Q., Tremblay, J., Verbrugge, C., 2014. Generative methods for guard and camera placement in stealth games, in: *Proceedings of the AAAI Conference on Artificial Intelligence and Interactive Digital Entertainment*, pp. 87–93.
- [50] Xu, Y., Wang, Y., Yang, J., Zhang, J., 2025. Two-stage terrestrial laser scan planning framework for geometric measurement of civil infrastructures. *Measurement* 242, 115785.
- [51] Zeng, Y., Liu, J., Cao, Q., Wu, Z., Chen, B., Li, D., Cheng, G., 2022. Optimal planning of indoor laser scans based on continuous optimization. *Automation in Construction* 143, 104552.
- [52] Zhai, R., Zou, J., Gan, V.J., Han, X., Wang, Y., Zhao, Y., 2024. Semantic enrichment of bim with indoorgml for quadruped robot navigation and automated 3d scanning. *Automation in Construction* 166, 105605.
- [53] Zhang, H., Yao, Y., Xie, K., Fu, C.W., Zhang, H., Huang, H., 2021. Continuous aerial path planning for 3d urban scene reconstruction. *ACM Trans. Graph.* 40, 225–1.
- [54] Zhang, W., Chen, Z., Huang, R., Dong, Z., Jiang, L., Xia, Y., Chen, B., Wang, H., 2023. Multiobjective optimization-based terrestrial laser

scanning layout planning for landslide monitoring. *IEEE Transactions on Geoscience and Remote Sensing* 61, 1–15.

- [55] Zhao, J., Yoshida, R., Cheung, S.c.S., Haws, D., 2013. Approximate techniques in solving optimal camera placement problems. *International Journal of Distributed Sensor Networks* 9, 241913.
- [56] Zheng, J., Zhang, J., Li, J., Tang, R., Gao, S., Zhou, Z., 2020. Structured3d: A large photo-realistic dataset for structured 3d modeling, in: *Proceedings of The European Conference on Computer Vision (ECCV)*.